Chapter 3

Optimized Solution

3.1 Introduction

As indicated in the previous chapters, various numerical strategies have been employed for reducing 1-port and 2-port scattering data for both nonmagnetic and magnetic materials. The vast majority of the work in this area has involved the determination of permittivity and permeability by the reduction of scattering data frequency by frequency, that is, by the explicit or implicit solution of a system of nonlinear scattering equations at each frequency (see [11,33]; as an example of a multifrequency approach see Maze et al.[15]).

What is lacking in the literature are practical, robust, numerical reduction techniques for more accurate determination of permittivity and permeability in transmission lines. Reliable broadband permeability and permittivity results for low-loss, medium-to-high dielectric constant materials are hard to obtain with transmission line techniques. Coaxial line measurements are particularly hard to obtain due to air gap influences and overmoding. Traditional transmission line numerical techniques have difficulties to an extent that render these techniques of limited use for low-loss materials and for high dielectric constant materials. Difficulties arise with these methods for magnetic materials in that numerical singularities can occur at frequencies corresponding to integral multiples of one half wavelength. These instabilities arise from the fact that for low-loss materials both S_{21} and S_{11} become equations for the phase velocity, and the permittivity and permeability therefore enter as a product. These instabilities limit the acquisition of precise broadband dielectric and magnetic results in the neighborhood of a resonance. Another problem pertains to high dielectric constant materials. High dielectric constant materials are usually hard to measure since the theoretical models are limited to a single, fundamental mode and the data contain both fundamental and higher order mode responses. Further, point-by-point reduction techniques for magnetic materials contain large random uncertainties due

to the propagation of uncertainties through the equations. For nonmagnetic materials the propagation of errors is less of a problem.

In our search for better reduction techniques we have found that nonlinear optimization, which minimizes the squared error, are a viable alternative solution. Optimization-based data reduction has an advantage over point-by-point schemes in that correlations are allowed between frequency measurements. In nonlinear regression, if deemed appropriate, it is not necessary to even include S_{11} data in the constraint equations. Another advantage of regression is that constraints such as causality and positivity can be incorporated into the solution.

This chapter presents a method for obtaining complex permittivity and permeability spectra from scattering parameter data on isotropic, homogeneous materials using nonlinear regression. We solve the scattering equations in a nonlinear least-squares sense with a regression algorithm over the entire frequency measurement range. The complex permittivity and permeability are obtained by determining estimates for the coefficients of a truncated Laurent series expansion for these parameters consistent with linearity and causality constraints. The procedure has been successfully used for accurate permittivity and permeability characterization of a number of different samples where point-by-point schemes have proven to be inadequate. The details of the numerical method have been presented in [36]. The problem applied to microwave measurements is presented in this chapter. The method can easily be extended to the analysis of multi-mode problems and the determination of experimental systematic uncertainty. The novel features of our algorithm are:

- The algorithm finds a "best fit" to the 2-port scattering equations using a nonlinear least-squares solution for the permittivity and permeability.
- The algorithm uses fitting functions that satisfy causality requirements.
- The numerical technique allows slight variations in the sample and reference position lengths to compensate for measurement errors and sample imperfections.
- The method allows the de-emphasis of frequency points with large phase uncertainty.
- Statistics related to the solution parameters are automatically generated.
- The technique can force positivity of the fit functions.
- It is possible to determine both complex permittivity and permeability from measurements of a single scattering parameter on a 1-port or a 2-port taken over a frequency band.

3.2 Model for Permeability and Permittivity

In the optimization procedure the S-parameter eqs (2.31) through (2.33) for single-mode problems, or eqs (2.21) through (2.24) for problems with higher order modes are solved for the material parameters by the optimization routine. For higher order mode problems the matrix elements A_{jk} in eqs (2.21) through (2.24), which corresponds to the voltage in each mode, can be determined by the optimization routine. However, we usually consider only the primary mode.

The unknown quantities are L_1, L_2, L, λ_c, and $\mu_R^*(\omega)$ and $\epsilon_R^*(\omega)$. Some of these parameters, such as the lengths and cutoff wavelength, are known accurately within measurement uncertainty. Obviously the parameters of interest cannot be allowed to vary into non-physical realms. The problem is to use an optimization routine to determine the model parameters that are consistent with the scattering data and the physics of the problem.

3.2.1 Relaxation Phenomena in the Complex Plane

The numerical model requires an explicit functional form for μ_R^* and ϵ_R^* to reproduce the four S-parameters consistent with the data, for all the n frequency observations.

The general form for $\mu_R^*(\omega)$ and $\epsilon_R^*(\omega)$ should be causal see Appendix C; that is, it must satisfy a Kramers-Kronig relation. If the zeros and poles of a complex function are known over the complex plane, the function itself is known.

The Laplace transform of the real, time-dependent permittivity satisfies

$$\epsilon(\vec{r}, s) = \int_0^\infty \epsilon(\vec{r}, t) e^{-st} dt \ . \tag{3.1}$$

For stability, there can be no poles in the right-half side of the s-plane. Since $\epsilon(t)$ is real it can be shown that the poles and zeros are confined to the negative real s-axis of the s-plane, and the poles which are off the real s- axis must occur in complex conjugate pairs [37].

Assuming linear response a constitutive relationship in an isotropic medium between the displacement and electric fields is

$$\vec{D}(\vec{x}, t) = \epsilon_0 \vec{E}(\vec{x}, t) + \epsilon_0 \int_0^\infty G(\tau) \vec{E}(\vec{x}, t - \tau) d\tau \ . \tag{3.2}$$

With this definition the permittivity is

$$\epsilon_R^*(\omega) = 1 + \int_0^\infty G(\tau) \epsilon^{-j\omega\tau} d\tau \ . \tag{3.3}$$

The response function $G(\tau)$ for an incident electric field can sometimes be represented as a series of damped sinusoids of the form

$$G(t) = \sum_n A_n \exp(-(a_n + jb_n)t) \ . \tag{3.4}$$

We assume that the material parameters can be adequately modeled by a series of simple poles. The terms $e^{-a_n t}$ relate to relaxation and the terms $e^{-jb_n t}$ relate to resonant phenomena. Since the Laplace transform of eq (3.4) is

$$G(s) = \sum_n A_n \frac{1}{s + a_n + jb_n} \ , \tag{3.5}$$

for stability (no increasing time domain exponentials) there can be no poles or zeros in the right half-side of the s-plane [37], [38]. In order to maintain the reality of $\epsilon(s)$, any poles off the imaginary axis in the ω-plane must be conjugate poles of the form $\omega = ja \pm b$ where a and b are real, positive numbers as indicated in figure 3.1. These conjugate poles are of the form

$$\frac{1}{s + a + jb} + \frac{1}{s + a - jb} \ , \tag{3.6}$$

and are related to resonant phenomena.

We assume that the permittivity can be expressed as

$$\epsilon_R^* = C \left[\prod_n \frac{(j\omega + z_n)}{(j\omega + p_n)} + \sum_n [\frac{1}{j\omega + a_n + jb_n} + \frac{1}{j\omega + a_n - jb_n}] \right] \ . \tag{3.7}$$

Here z_n and p_n are the zeros and poles due to damped exponentials respectively, $(a_n \pm jb_n)$ are the complex conjugate poles, and C is a complex constant.

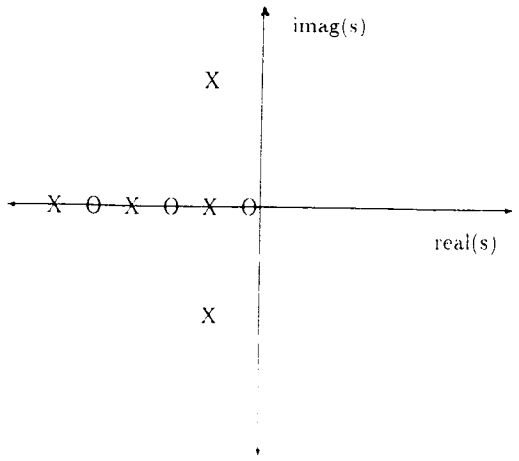

Figure 3.1: Poles (X) and zeros (O) in the complex s-plane and conjugate poles off the real s-axis.

For more complicated polarization phenomena other relations for permittivity could be used. For a continuous distribution of relaxation times

$$\epsilon' = \epsilon_\infty + [\epsilon(0) - \epsilon_\infty] \int_0^\infty \frac{y(\tau)}{1 + \omega^2\tau^2} d\tau \ , \tag{3.8}$$

$$\epsilon'' = [\epsilon(0) - \epsilon_\infty] \int_0^\infty \frac{\omega\tau y(\tau)}{1 + \omega^2\tau^2} d\tau \ , \tag{3.9}$$

where $y(\tau)$ is a distribution function. Various expressions for y yield various relations for permittivity. Presently we use eqs (3.11) and (3.12) in our calculations. The Havriliak-Negami model for materials assumes a single nonsimple pole on the negative, real s-plane axis:

$$\epsilon_R^* = C + \frac{A}{(1 + [j|B|\omega]^{1-\alpha})^\beta} \ , \tag{3.10}$$

where β and α are in the interval $[0, 1]$ and B is real. Limiting cases of this model are (1) the Cole-Davidson model when $\alpha = 0$; this model works well for some liquids and solid polymers, (2) the Cole-Cole model when $\beta = 1$; this model has been used to describe relaxation behavior of amorphous solids and many liquids. A simple Debye model ($\beta = 1$ and $\alpha = 1$) is very limited and works well only for materials that contain a single relaxation time in the frequency range of interest.

Heterogeneous materials and polymers usually have a very broad relaxation spectrum and as such have a response of the form of a power law such as s^{-a}. This behavior can be obtained from the Cole-Davidson model when $|B|\omega >> 1$.

In our present algorithm we assume a more general model than the single Debye relaxation model a truncated Laurent series is used for $\mu_R^*(\omega)$ and $\epsilon_R^*(\omega)$. This expansion has

generally yielded excellent results

$$\mu_R^*(\omega) = A_0 + \frac{A_1}{1 + j|B_1|\omega} + \frac{A_2}{(1 + j|B_2|\omega)^2} \ , \tag{3.11}$$

$$\epsilon_R^*(\omega) = D_0 + \frac{A_3}{1 + j|B_3|\omega} + \frac{A_4}{(1 + j|B_4|\omega)^2} \ , \tag{3.12}$$

where B_i are real numbers. The pole information yields constraints on the constants used in the Laurent series expansion. For example, it is required that B_i is a real number.

For a typical measurement on a network analyzer there may be 400 frequency points and at each point all four scattering parameters are taken. The problem is overdetermined since for n frequency measurements, if we assume known lengths, there are $8n$ real equations for the unknown quantities in the Laurent series. This over determination can be used at frequencies in the gigahertz range to find corrections to sample position and cut off wavelength.

The approach for determining the complex parameters A_j, B_j is to minimize the sum of the squares of the differences between the predicted and observed S-parameters,

$$\min \| \sum_{ij} \vec{S}_{ij} - \vec{P}_{ij} \| \ , \tag{3.13}$$

where the measured vectors are denoted by $\vec{S}_{ij} = (S_{ij}(\omega_1), S_{ij}(\omega_2), .., S_{ij}(\omega_n))$ and where $\vec{P}_{ij}$ is the predicted vector. Hence, the problem consists of finding the norm solution to these equations.

3.3 Numerical Technique

3.3.1 Algorithm

The solution currently uses a software routine called orthogonal distance regression pack ODRPACK [39] developed at the National Institute of Standards and Technology. This routine is an extended form of the Levenberg-Marquardt approach. This procedure allows for both ordinary nonlinear least-squares, in which the uncertainties are assumed to be only in the dependent variable, and, orthogonal distance regression, where the uncertainties appear in both dependent and independent variables. First-order derivatives for the Jacobian matrices can be numerically approximated (finite difference approximation) or can be user-supplied analytical derivatives. The procedure performs automatic scaling of the variables if necessary, as well as determining the accuracy of the model in terms of machine precision. The trust region approach enables the procedure to adaptively determine the region in which the linear approximation adequately represents the nonlinear model.

Iterations are stopped by ODRPACK when any one of three criteria are met. These criteria are: (1) the difference between observed and predicted values is small, (2) the convergence to a predicted value is sufficiently small, and (3) a specified limit on the number of iterations has been reached.

Initial guesses for ϵ_R^* and μ_R^* are obtained from explicit solutions of Stuchly [7] or Weir [6]. The most significant input parameters for modeling permittivity and permeability are the initial values for A_i and B_i. Sensitivity to the initial solution for these parameters is discussed below. All additional parameters are initialized to 0.

When measurements of length and scattering parameters of a sample are taken, there are systematic uncertainties.

An orthogonal distance regression model provides the modeler with the additional ability to assume that the independent variable, in this case, frequency, may contain some uncertainty as well. Allowances for these types of uncertainty can, in some cases, greatly improve the approximation. For this model and the samples tested, the errors in the independent variables are sufficiently small that an ordinary least-squares approximation is adequate.

Model parameters such as sample length, sample position in the waveguide, and cutoff wavelength could contain a systematic uncertainty. These parameters were allowed to vary over a limited region, and the optimization procedure chooses optimum values for the parameter. This procedure assumes that systematic measurement errors can be detected by the routine. For example, inserting a sample into a sample holder introduces an uncertainty in the sample position L_1, so we include with L_1 an additional optimization parameter β_{L1} in R_1 to account for positioning uncertainties,

$$R_1 = \exp(-\gamma_o[L_1 + \beta_{L1}]) \ . \tag{3.14}$$

Also for R_2

$$R_2 = \exp(-\gamma_o[L_2 + \beta_{L2}]) \ . \tag{3.15}$$

The routine requires that the length corrections be within a prescribed range which represents physical measurement uncertainty. The length of the sample L is completely determined by

$$L = L_{air} - (L_1 + L_2 + \beta_{L1} + \beta_{L2}) \tag{3.16}$$

and is also implicitly parameterized by the values of β_{L1} and β_{L2}.

Due to inaccuracies in machining of the sample holder there is an uncertainty in the cutoff wavelength of the guide. We account for this by the introduction of an additional optimization parameter $\lambda_c \rightarrow \lambda_c + \beta_\lambda$. We constrain this variation to be within measurement accuracy.

The model can use various combinations of the available data to estimate both the relative permeability and permittivity from scattering data. For example, S_{21} or S_{11} alone

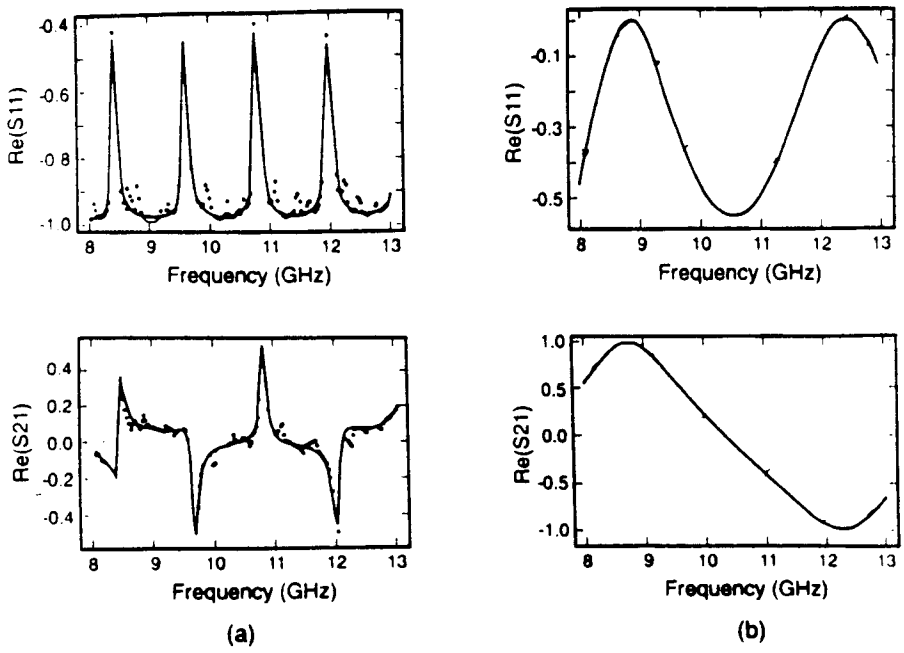

Figure 3.2: Predicted (solid line) and observed (dots) parameters for a barium titanate compound (a) and cross-linked polystyrene in (b).

can be used to obtain both permeability and permittivity. This can be contrasted with point-by-point techniques where both S_{21} and S_{11} are required. Also, magnitude alone can similarly be used. Magnitude data have the advantage of requiring no reference plane rotation.

The technique works well for short-circuit line measurements. For short-circuit lines it is possible with this technique to obtain both the complex permittivity and permeability from a single broadband measurement on one sample at a single position in the line.

3.3.2 Numerical Results

The model predictions are formed by inserting eqs(3.11) and (3.12) into (2.31) and (2.33) or (4.7) and then finding the unknown coefficients in the equations for ϵ_R^* and μ_R^* that produces the least square error. In figure 3.2 the experimental results are given for a barium titanate compound and cross-linked polystyrene. These samples required 21 and 40 iterations respectively.

The difference between the predicted S-parameter and the observed values reveals the presence of systematic uncertainty, as shown in figure 3.3, in the automatic network analyzer (ANA). Additional tests revealed the source of the systematic error did not appear to be related to the material tested in the waveguide. In fact, uncertainties produced for the cross-linked polystyrene sample closely resemble the S-parameter data for an empty waveguide;

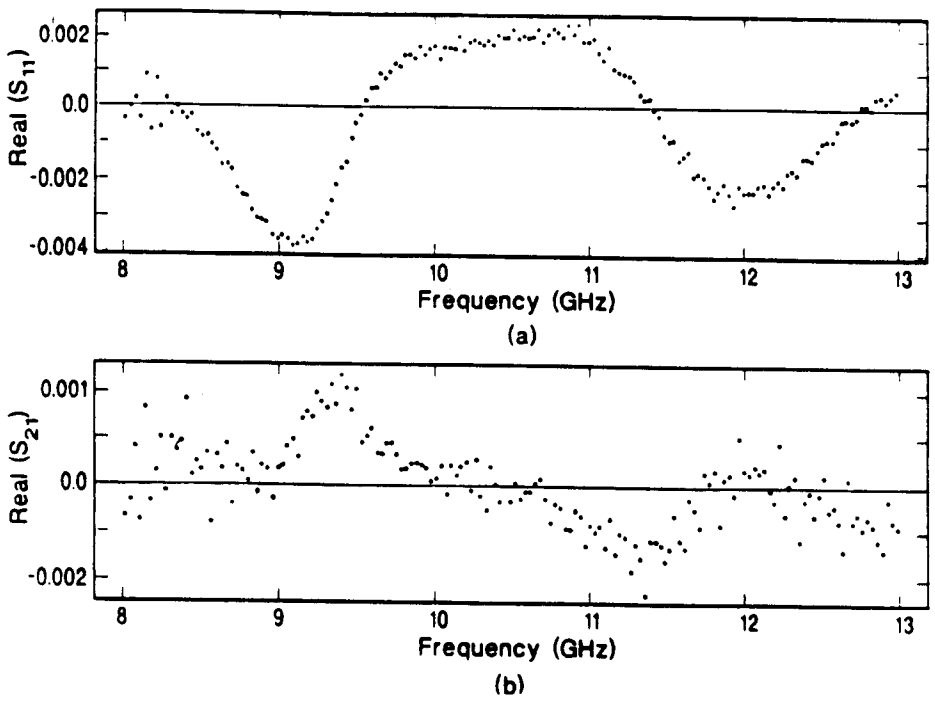

Figure 3.3: Systematic uncertainty as indicated by the residual plot (the difference betweer the observed and predicted values) for the case on an empty waveguide. The solid line is at 0 residual.

we conclude therefore that much of the systematic error is due to calibration uncertainty and joint losses at connector interfaces. For the barium titanate compound sample there is both the fundamental mode response and smaller resonances related to higher-order modes. As shown in figure C.1, the model interpolates a fundamental mode. This raises the possibility of extending the model to incorporate higher-order modes by extending the theoretical formulation of the problem.

It is easy to move the sample in the holder inadvertently when connecting the sample holder to the port cables. Positioning errors of the sample in the air line can result in large error in computed material parameters. The numerical algorithm can adjust for positioning errors by adjusting L_1 or L_2 slightly. The effects of positioning error can be seen in figure 3.4.

In this example the routine predicted that the position of the sample was off by 0.8 mm.

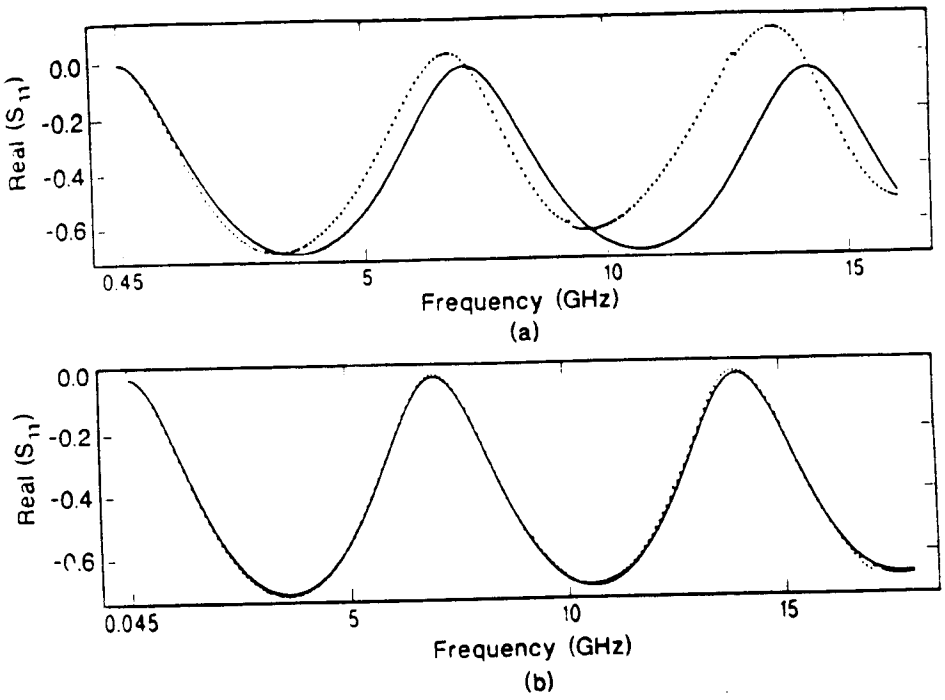

Figure 3.4: Measured real part of S_{11}, measured (. . . .) and predicted (———), for a glass sample (a) with positioning error for L_1 and (b) the solution when the algorithm adjusts for the positioning error.

3 4 Permittivity and Permeability

3.4.1 Measurements

In this section we present the measured and calculated permittivity and permeability. Cross-linked polystyrene and the barium titanate compound are nonmagnetic and therefore $\mu_R^* = 1$. Comparison of the optimized solution to a point-by-point solution is shown in figure 3.5. In figures 3.6 through 3.9 results for four samples are given.

As a check we made an independent measurement of the barium titanate compound in an X-band cavity where the results were $\epsilon_R' = 269$ at 10 Ghz. This result can be compared to the results in figure 3.6. Finally a result of another barium titanate compound is given below.

3.4.2 Robustness of the Procedure

Since the transmission coefficient contains a periodic component, there is more than one solution to the system of equations. Each root of the equation has a neighborhood around which convergence will occur for initial guesses in that region. The robustness of a mathematical procedure is related to how well the algorithm treats the neighborhood around the

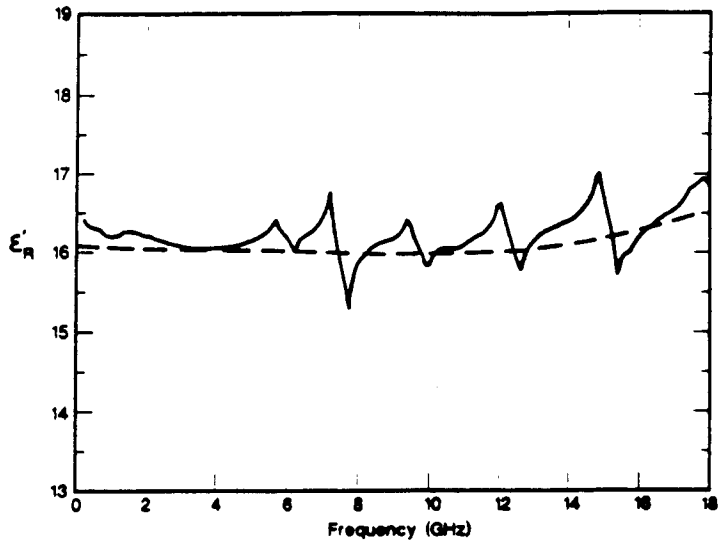

Figure 3.5: Permittivity in the frequency range of $0.045 - 18$ Ghz for the optimized solution (- - - -) and point-by-point technique (——).

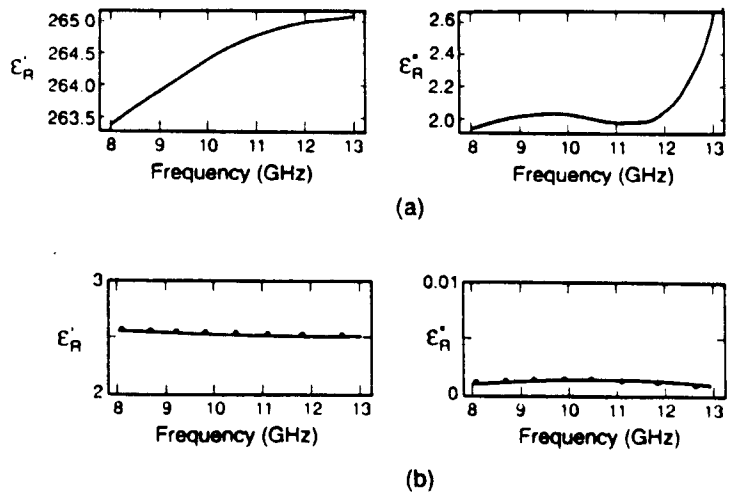

Figure 3.6: Permittivity for barium titanate compound (a) and cross- linked polystyrene (b), point-by-point method (. . . .), optimized solution (—-).

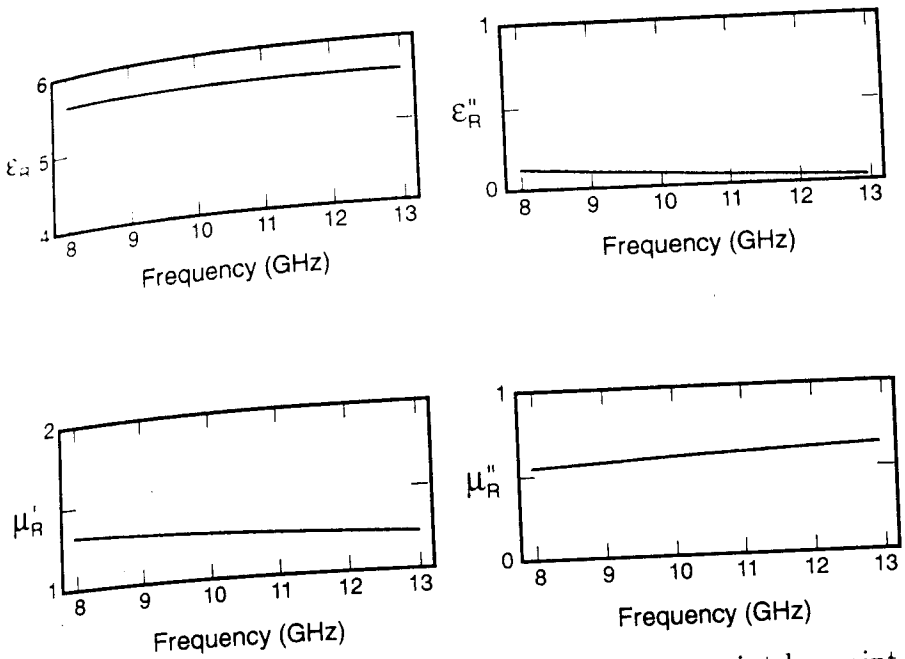

Figure 3.7: Permittivity and permeability for a loaded-polymer, point-by-point method (. . . optimized solution (——-).

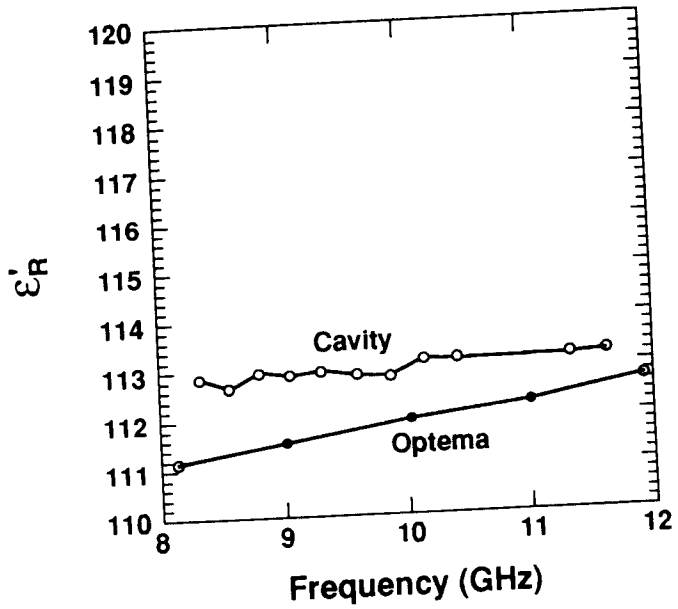

Figure 3.8: Real part of permittivity for a barium titanate compound (o o o) cavity (. . .) optimized solution.

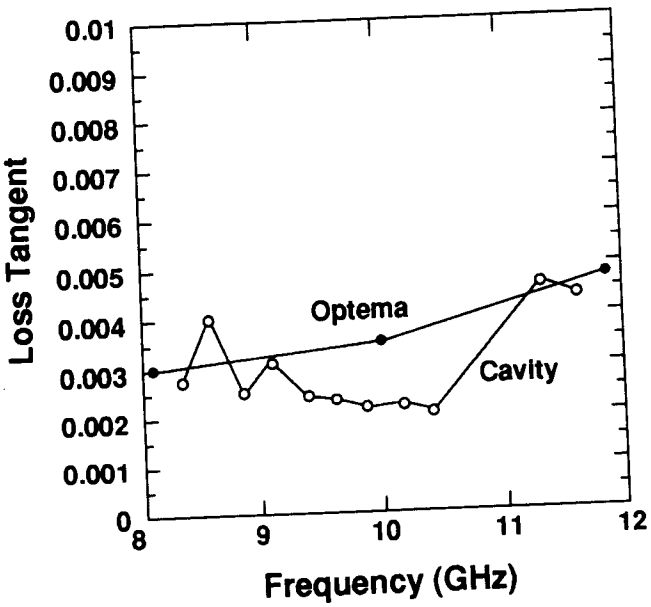

Figure 3.9: Imaginary part of permittivity for a barium titanate compound o o o -cavity and . . . - optimized solution.

correct root. The existence of alternative optima in the mathematical model requires an accurate initial guess in order to converge to the correct solution. Typically convergence occurs after about seven iterations. The use of constraints and the large number of equations enhances the uniqueness of the solution by reducing the dimensions of the solution space.

In point-by-point methods the correct solution is selected from the infinity of possible roots by calculating the slope of the phase curve and comparing the measured and calculated group delays. A group delay constraint is also used as a way of determining the physical solution.

The numerical effectiveness of the entire permeability and permittivity calculation depends on the robustness of the ODRPACK procedure and, more significantly, the robustness of the mathematical model. For the samples used in this study, the robustness of the procedure depended on the sample. For the materials with low dielectric constant the procedure readily determined a solution for a variety of input values with a large radius of convergence. For materials with higher dielectric constant, the procedure often converged quickly, although the existence of alternative local optima in the mathematical model required some testing to make sure that the converged root was the correct root.

3.5 Discussion

An optimization approach to the solution of the scattering equations appears to be a viable alternative to point-by-point techniques. The technique allows a stable solution for a broad range of frequencies. The method works particularly well for short-circuit line measurements. Unlike the point-by-point short-circuit method which requires measurements on two samples or in two positions, the optimized solution can obtain complex permittivity and permeability on a single sample at a single position.

The reflection (S_{11}) data are usually of lesser quality than the transmission data (S_{21}) for low-loss, low- permittivity materials. Therefore S_{11} need not be included in the solution for low-loss materials. However, reflection data S_{11} and S_{22} are very useful in determining the position of the sample in the air line as indicated in figure 3.7. The technique was successful for many isotropic magnetic and relatively high dielectric constant materials. The addition of constraints to the solution is powerful in that it further limits the possible solution range of the system of equations and enhances the uniqueness of the solution. The use of analytic functions for the expansion functions allows a correlation between the real and imaginary parts of the permittivity and permeability. The results shown in figures 3.5 through 3.6 indicate that the method can be used to reduce scattering data of fairly high dielectric constant materials. In fact, in some cases the optimized procedure yields solutions when the point-by-point technique fails completely.

Why does an optimization approach, in many cases, reliably reduce data on higher dielectric constant materials ($\epsilon'_R > 20$), whereas point-by-point techniques generally fail? Scattering data for higher dielectric constant materials contain responses to both primary mode and higher order modes. As indicated in figure 3.2 for the barium titanate compound, the optimization routine selects the primary mode data and places less weight on the higher mode resonance data.

The optimized technique can be used to treat problems where sample lengths, sample holder lengths, and sample positions are not known to high accuracy. Permittivity and permeability can be found from the equations without specifying either sample position or sample length. This result could find application to high-temperature measurements.

Higher-order modes propagate in samples when two conditions are met. The frequencies must be above cutoff in the sample, and there must be inhomogeneities or asymmetries in the sample to excite the higher order modes. Higher-order modes can be incorporated into this type of model by letting the optimization routine select the power in each mode. Higher-order mode models are a subject of our current research.

Chapter 4

Short-Circuit Line Methods

4.1 Theory

In this section we review the mathematical formalism for short-circuit measurements. We consider a measurement of the reflection coefficient (S_{11} for a shorted two-port) as a function of frequency. We begin with a mathematical analysis of the electromagnetic fields in the sample. The details of the field model have been presented previously [26] and only the most essential details will be presented here.

Assumptions on the electric fields in regions I, II, and III shown in figure 4.1 may be made as follows: (1) only the dominant mode is present in the waveguide; (2) the materials are homogeneous and isotropic; (3) only transverse electric fields are present. Under these conditions the electric fields in these regions may be expressed as:

$$E_I = \exp(-\gamma_0 z) + S_{11} \exp(\gamma_0 z) \ , \tag{4.1}$$

$$E_{II} = C_2 \exp(-\gamma z) + C_3 \exp(\gamma z) \ , \tag{4.2}$$

$$E_{III} = C_4 \exp(-\gamma_0 (z - L)) + C_5 \exp(\gamma_0 (z - L)) \ . \tag{4.3}$$

We wish to determine the coefficients in eqs (4.1) through (4.3) by imposing boundary conditions on the system of equations. The boundary conditions are:

- Tangential component of the electric field is continuous at sample interfaces.
- Tangential component of the magnetic field is continuous at sample interfaces.
- The electric field is null at the short-circuit position (perfect reflect).

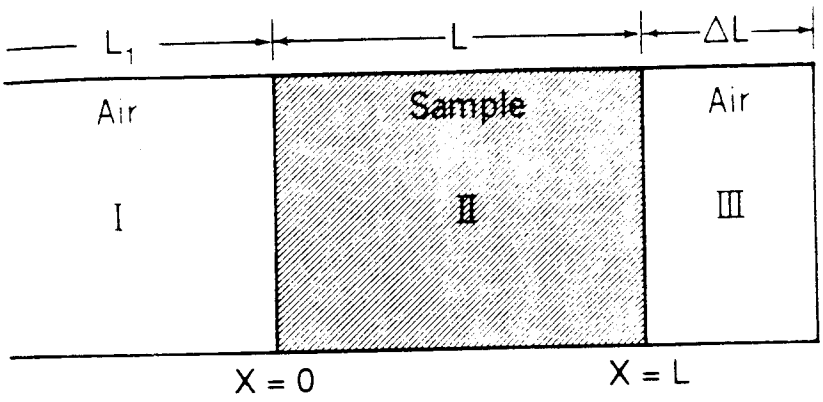

Figure 4.1: A transmission line with a short-circuit termination.

Expressions for the coefficients in eqs (4.1) through (4.3) are presented in reference [26].

Matching boundary conditions of the field equations at the interface and the reflect yields an equation for the permittivity and permeability in terms of the reflection coefficient, $\rho = S_{11} = C_1$. With the sample end face located a distance ΔL from the short,

$$S_{11} = \rho = \frac{-2\beta\delta + [(\delta+1) + (\delta-1)\beta^2]\tanh\gamma L}{2\beta + [(\delta+1) - (\delta-1)\beta^2]\tanh\gamma L} , \tag{4.4}$$

where

$$\beta = \frac{\gamma\mu_o}{\gamma_o\mu} , \tag{4.5}$$

and

$$\delta = \exp(-2\gamma_o\Delta L) . \tag{4.6}$$

In terms of hyperbolic functions

$$S_{11} = \frac{\tanh\gamma L + \beta\tanh\gamma_0\Delta L - \beta(1 + \beta\tanh\gamma L\tanh\gamma_0\Delta L)}{\tanh\gamma L + \beta\tanh\gamma_0\Delta L + \beta(1 + \beta\tanh\gamma L\tanh\gamma_0\Delta L)} . \tag{4.7}$$

S_{11} for a matched two-port can be obtained as a special case from eq (4.4) by letting $\delta \to 0$.

Although in the derivation of eq (4.7) it is assumed that the sample plane coincides with the measurement calibration plane, this is not the case in general; however, we can transform the reference plane position by a simple procedure. To accomplish this, we write the most general expression for the reflection coefficient as

$$S_{11(trans)} = R_1^2 S_{11} \ , \tag{4.8}$$

where $S_{11trans}$ is the reflection coefficient at the calibration reference plane position,

$$R_1 = \exp(-\gamma_o L_1) \ , \tag{4.9}$$

and L_1 is the distance from the calibration plane to the sample front face. Equation (4.8) transforms the reflection coefficient from the calibration plane to the plane of sample front face. It is of interest in many applications to eliminate the distance L_1 from eq (4.8). This can be accomplished by measuring S_{11} of the empty sample holder,

$$S_{11(empty)} = -\exp(-2\gamma_o[L_1 + \Delta L + L]) = -\exp(-2\gamma_0 L_{air}) \ , \tag{4.10}$$

and therefore the ratio of the filled to empty holder reflection coefficient is

$$\frac{S_{11(trans)}}{S_{11(empty)}} = -\exp(2\gamma_0[\Delta L + L])S_{11} \ . \tag{4.11}$$

If both the permeability and the permittivity are required, measurement data for two different short-circuit positions are needed. Note that standing waves can be formed in the region between the sample and short-circuit and between the calibration plane and sample front-face. Therefore certain frequencies, depending on sample length and the other lengths, will give better results for permittivity and other frequencies better results for permeability.

The position of the short-circuit is a low electric field and high magnetic field region and a position $\lambda/4$ from the short- circuit is a high electric field and low magnetic field region. Therefore as frequency permits, for permittivity measurements the sample should be moved away from the short-circuit termination. Permeability in isolation can be obtained with the sample at the short-circuit position. Of course when an ANA is used measurements will be taken at many combinations of field strengths and therefore the uncertainty will vary with frequency.

4.1.1 Two Samples of Different Lengths

It is possible to solve for the permeability and permittivity when the scattering parameters with samples of two differing lengths are measured. To see this, let us consider two samples, one of length L and one of length αL as indicated in figure 4.2.

Then for independent measurements on the two samples we have

$$S_{11(1)} = \frac{\Gamma - Z^2}{1 - \Gamma Z^2} \ , \tag{4.12}$$

and

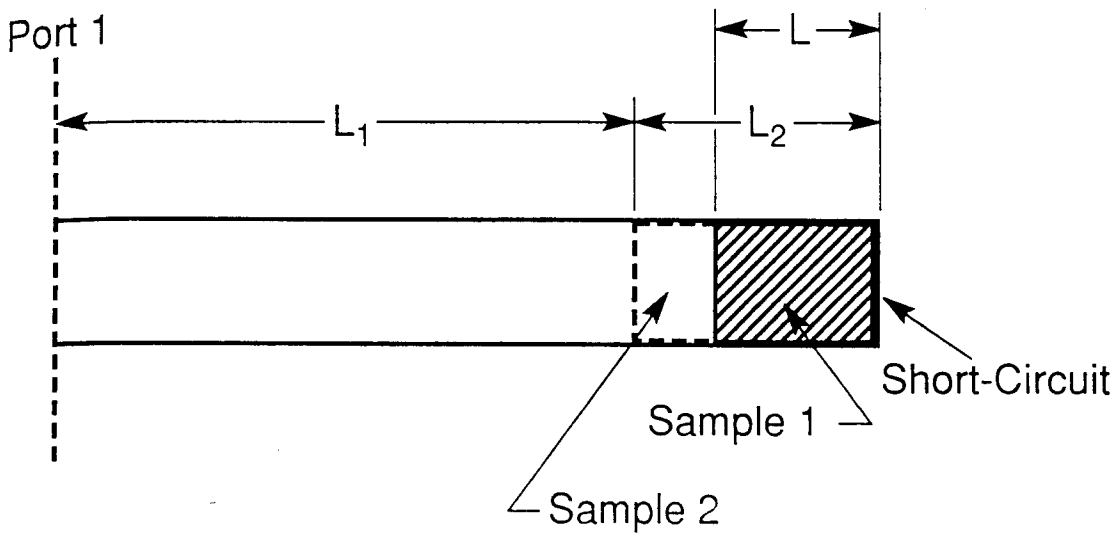

Figure 4.2: A transmission line with a short-circuit termination in two sample magnetic measurements.

$$Z = \exp(-\gamma L) \ . \tag{4.13}$$

The reflection coefficient Γ is given by eq (2.37). The scattering 1-port parameter is given by

$$S_{11(2)} = \frac{\Gamma - Z^{2\alpha}}{1 - \Gamma Z^{2\alpha}} \ . \tag{4.14}$$

Therefore we can solve for Z in eq (4.12),

$$Z^2 = \frac{S_{11(1)} - \Gamma}{S_{11(1)}\Gamma - 1} \ , \tag{4.15}$$

and substitute it into eq (4.14) to obtain

$$S_{11(2)} = \frac{\Gamma - \left[\frac{S_{11(1)}-\Gamma}{S_{11(1)}\Gamma-1}\right]^{\alpha}}{1 - \Gamma\left[\frac{S_{11(1)}-\Gamma}{S_{11(1)}\Gamma-1}\right]^{\alpha}} \ . \tag{4.16}$$

Equation (4.16) is solved iteratively for Γ and then Z is found from eq (4.15). The permittivity and permeability can then be obtained, if we define

$$\frac{1}{\Lambda^2} = -[\frac{1}{2\pi L}\ln(\frac{1}{Z})]^2 \ , \tag{4.17}$$

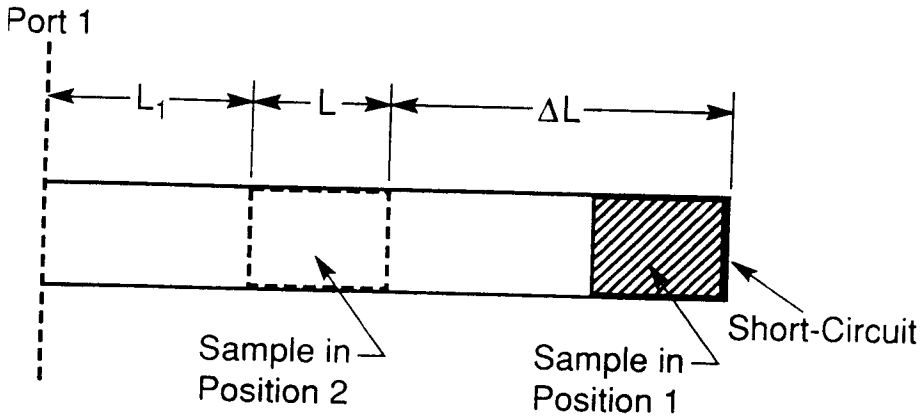

Figure 4.3: A transmission line with a short-circuit termination for two-position measurements.

$$\epsilon_R^* = \frac{\lambda_0^2}{\mu_R^*}\left[\frac{1}{\lambda_c^2} - \frac{1}{\Lambda^2}\right], \tag{4.18}$$

$$\mu_R^* = \frac{1+\Gamma}{(1-\Gamma)\Lambda\sqrt{\frac{1}{\lambda_0^2} - \frac{1}{\lambda_c^2}}}, \tag{4.19}$$

where λ_0 is the free-space wavelength and λ_c is the cutoff wavelength. Equation (4.17) has an infinite number of roots for magnetic materials because the logarithm of a complex number is multi-valued. In order to pick out the correct root it is necessary to compare the measured to the calculated group delay.

4.1.2 Single Sample at Two Short-Circuit Positions

It is possible to obtain an explicit solution to eq (4.4) when measurements at two different short-circuit positions are taken. The explicit solution is obtained by solving eq (4.4) at a given short-circuit position (position 1) for $\tanh\gamma L$ and then substituting this expression into eq (4.4) at another short-circuit position (position 2) as indicated in figure 4.3.

For two different short-circuit positions at the same frequency we obtain ρ_1 and ρ_2 for positions 1 and 2:

$$\rho_1 = \frac{2\beta\delta_1 - [(\delta_1+1)+(\delta_1-1)\beta^2]\tanh\gamma L}{-2\beta + [(\delta_1-1)\beta^2 - (\delta_1+1)]\tanh\gamma L}\ , \tag{4.20}$$

$$\rho_2 = \frac{2\beta\delta_2 - [(\delta_2+1)+(\delta_2-1)\beta^2]\tanh\gamma L}{-2\beta + [(\delta_2-1)\beta^2 - (\delta_2+1)]\tanh\gamma L}\ , \tag{4.21}$$

where δ_1, δ_2 denote the phases calculated from eq (4.6) for $\Delta L_1, \Delta L_2$ respectively. These equations yield

$$\tanh\gamma L = \frac{2\beta(\delta_1+\rho_1)}{\beta^2(\rho_1+1)(\delta_1-1)+(1-\rho_1)(\delta_1+1)}\ , \tag{4.22}$$

$$\gamma = \frac{1}{L}\left(\tanh^{-1}\left[\frac{2\beta(\delta_1+\rho_1)}{\beta^2(\rho_1+1)(\delta_1-1)+(1-\rho_1)(\delta_1+1)}\right] + 2n\pi j\right)\ , \tag{4.23}$$

where n is an integer. Since the arctangent is multi-valued, the correct value of n is determined from the group delay arguments given in section 3.2.1. Also

$$\beta^2 = \frac{\delta_1(\delta_2(\rho_1-\rho_2)+\rho_1\rho_2+1-2\rho_2) - (\delta_2(\rho_1(\rho_2-2)+1)+\rho_2-\rho_1)}{\delta_1(\delta_2(\rho_1-\rho_2)+\rho_1\rho_2+1+2\rho_2) - (\delta_2(\rho_1(\rho_2+2)+1)+\rho_2-\rho_1)}\ . \tag{4.24}$$

Once β is known, eqs(4.22) and (4.24) can be used to find permittivity and permeability.

4.2 Measurements

In the SCL technique the scattering parameter S_{11} is measured broadband, with the sample at a given position in the sample holder. The distance from the sample to the short-circuit termination must be known to a high degree of accuracy. If both permeability and the permittivity are required then the sample must be moved in the line and the S-parameters again taken.

Depending on the position of the short-circuit, the sample may be immersed in either a region of high electric field or high magnetic field. A strong electric field is advantageous for permittivity determination, whereas a strong magnetic field is advantageous for permeability determination. Generally, the sample end will be in a region of high magnetic field when the sample is in closest physical contact with the short. It is possible to take advantage of the fluctuating electric and magnetic field distributions when performing permittivity and permeability measurements. When taking broadband measurements on an ANA it is possible to predict when the sample is immersed in the various field strengths. Then one can select the measurements to be used for permittivity and permeability calculations [35].

Measurements were made on an ANA for various samples. Using eq (4.4) we obtain the permittivity and permeability which are shown in figures 4.4 and 4.5.

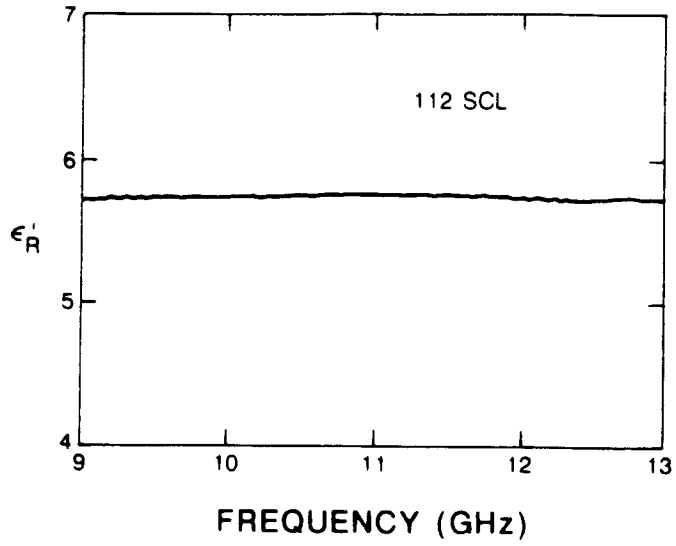

Figure 4.4: ϵ'_R without gap correction using SCL for a loaded polymer mixture.

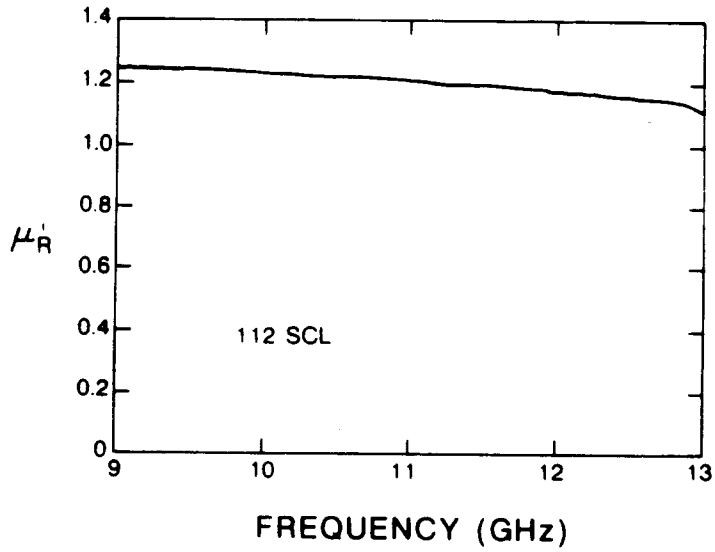

Figure 4.5: μ'_R without gap correction using SCL for a loaded polymer mixture.

4.3 Uncertainty of Short-Circuit Line Measurements

For magnetic materials it is necessary to make two independent measurements at a given frequency. Independent measurements can be obtained either by measuring samples of two different lengths or by taking measurements of a given sample at two locations in the line. The special case of measurement of two samples of varying lengths (L_1, L_2) can be obtained from the solution presented below by substituting $L \rightarrow L_1$, $\gamma_0 \rightarrow \gamma$ and $\Delta L \rightarrow L_2 - L_1$.

The uncertainty involved in two position measurements is explored in this section. The uncertainty incurred with the equations expounded in this report is estimated. The sources of uncertainty in the SCL measurement include

- Uncertainties in measurements of the magnitude and phase of the scattering parameters.
- Gaps between the sample and sample holder.
- Dimensional variations in the sample holder.
- Uncertainty in sample length.
- Short-circuit and line losses and connector mismatch.
- Uncertainty in positions of the reference plane and sample in holder.

Adjustment for errors due to gaps around the sample is obtained from equations available in the literature [33,34,35]. The formulas given in the literature generally under-correct for the real part of the permittivity and over-correct for the imaginary part of the permittivity. All measurements of permittivity are assumed to have been corrected for air gaps around the sample before the following uncertainty analysis is applied.

In order to evaluate the uncertainty introduced by the measured scattering parameters, we assume that a differential uncertainty analysis is applicable. This assumption implies that uncertainties are of small enough magnitude so that a local Taylor series can be applied. We assume that a Taylor series approximates deviations of the function from a given point. We assume that the worst case uncertainty due to the S-parameters and sample lengths can be written

$$\frac{\Delta\epsilon'_R}{\epsilon'_R} = \frac{1}{\epsilon'_R}\sqrt{\left(\frac{\partial\epsilon'_R}{\partial|S_{11}|}\Delta|S_{11}|\right)^2 + \left(\frac{\partial\epsilon'_R}{\partial\theta_{11}}\Delta\theta_{11}\right)^2 + \left(\frac{\partial\epsilon'_R}{\partial L}\Delta L\right)^2 + \left(\frac{\partial\epsilon'_R}{\partial d}\Delta d\right)^2}, \qquad (4.25)$$

$$\frac{\Delta\epsilon''_R}{\epsilon''_R} = \frac{1}{\epsilon''_R}\sqrt{\left(\frac{\partial\epsilon''_R}{\partial|S_{11}|}\Delta|S_{11}|\right)^2 + \left(\frac{\partial\epsilon''_R}{\partial\theta_{11}}\Delta\theta_{11}\right)^2 + \left(\frac{\partial\epsilon''_R}{\partial L}\Delta L\right)^2 + \left(\frac{\partial\epsilon''_R}{\partial d}\Delta d\right)^2}, \qquad (4.26)$$

where $\Delta\theta$ is the uncertainty in the phase of the scattering parameter, $\Delta|S_{11}|$ is the uncertainty in the magnitude of the scattering parameter, Δd is the uncertainty in the air gap around the sample, and ΔL is the uncertainty in the sample length. The gap correction uncertainty is given in [26]. The uncertainties used for the S-parameters depend on the specific ANA used for the measurements. In general uncertainties due to flange bolt torquing and connector repeatability must be added to these uncertainties.

Let us define the variables

$$a = \tanh \gamma L \ , \tag{4.27}$$

$$b = \tanh \gamma_0 \Delta L \ . \tag{4.28}$$

We wish to obtain explicit relations for the derivatives of ϵ_R^* and μ_R^* with respect to independent variables $|S_{11(i)}|$ and θ_i, $i = 1, 2$. We define $S_{11(1)}$ as the reflection at short position 1 and $S_{11(2)}$ as the reflection at short position 2. Next define

$$f = \frac{\tanh \gamma L + \beta \tanh \gamma_0 \Delta L - \beta(1 + \beta \tanh \gamma L \tanh \gamma_0 \Delta L)}{\tanh \gamma L + \beta \tanh \gamma_0 \Delta L + \beta(1 + \beta \tanh \gamma L \tanh \gamma_0 \Delta L)} - S_{11} = 0 \ . \tag{4.29}$$

We assume the following as independent variables $S_{11}(i)$, $i = 1, 2$, L, ΔL, and d. Derivatives of eq (4.29) with respect to the independent variables can be found analytically. By the chain rule we have

$$\underbrace{\left[\frac{\partial f}{\partial a}\frac{\partial a}{\partial \gamma}\frac{\partial \gamma}{\partial \mu_R^*} + \frac{\partial f}{\partial \beta}\frac{\partial \beta}{\partial \mu_R^*}\right]}_{a_1}\frac{\partial \mu_R^*}{\partial |S_{11}(m)|} + \underbrace{\left[\frac{\partial f}{\partial a}\frac{\partial a}{\partial \gamma}\frac{\partial \gamma}{\partial \epsilon_R^*} + \frac{\partial f}{\partial \beta}\frac{\partial \beta}{\partial \epsilon_R^*}\right]}_{a_2}\frac{\partial \epsilon_R^*}{\partial |S_{11}(m)|} = \exp(j\theta_m) \ , \tag{4.30}$$

This equation is evaluated at position one.

$$\underbrace{\left[\frac{\partial f}{\partial a}\frac{\partial a}{\partial \gamma}\frac{\partial \gamma}{\partial \mu_R^*} + \frac{\partial f}{\partial \beta}\frac{\partial \beta}{\partial \mu_R^*}\right]}_{b_{1m}}\frac{\partial \mu_R^*}{\partial |S_{11}(m)|} + \underbrace{\left[\frac{\partial f}{\partial a}\frac{\partial a}{\partial \gamma}\frac{\partial \gamma}{\partial \epsilon_R^*} + \frac{\partial f}{\partial \beta}\frac{\partial \beta}{\partial \epsilon_R^*}\right]}_{b_{2m}}\frac{\partial \epsilon_R^*}{\partial |S_{11}(m)|} = \exp(j\theta_m) \ . \tag{4.31}$$

This equation is evaluated at position two. The four derivatives can be written

$$a_1\frac{\partial \mu_R^*}{\partial |S_{11(m)}|} + a_2\frac{\partial \epsilon_R^*}{\partial |S_{11(m)}|} = \exp(j\theta_m)\delta_{1,m} \ , \tag{4.32}$$

$$b_1\frac{\partial \mu_R^*}{\partial |S_{11(m)}|} + b_2\frac{\partial \epsilon_R^*}{\partial |S_{11(m)}|} = \exp(j\theta_m)\delta_{2,m} \ , \tag{4.33}$$

where $\delta_{i,m}$ is the Kronecker delta function.

At the first position the derivatives with respect to length are

$$[\frac{\partial f}{\partial a}\frac{\partial a}{\partial \gamma}\frac{\partial \gamma}{\partial \mu_R^*} + \frac{\partial f}{\partial \beta}\frac{\partial \beta}{\partial \mu_R^*}]_m \frac{\partial \mu_R^*}{\partial L} + [\frac{\partial f}{\partial a}\frac{\partial a}{\partial \gamma}\frac{\partial \gamma}{\partial \epsilon_R^*} + \frac{\partial f}{\partial \beta}\frac{\partial \beta}{\partial \epsilon_R^*}]_m \frac{\partial \epsilon_R^*}{\partial L} + \frac{\partial f}{\partial a}\frac{\partial a}{\partial L} = 0 , \qquad (4.34)$$

or

$$a_1 \frac{\partial \mu_R^*}{\partial L} + a_2 \frac{\partial \epsilon_R^*}{\partial L} + \frac{\partial f}{\partial a}\frac{\partial a}{\partial L} = 0 , \qquad (4.35)$$

and for the second short-circuit termination position

$$b_1 \frac{\partial \mu_R^*}{\partial L} + b_2 \frac{\partial \epsilon_R^*}{\partial L} + \frac{\partial f}{\partial a}\frac{\partial a}{\partial L} = 0 . \qquad (4.36)$$

The derivatives with respect to the distance from the sample back face to the short-circuit termination can similarly be calculated

$$[\frac{\partial f}{\partial a}\frac{\partial a}{\partial \gamma}\frac{\partial \gamma}{\partial \mu_R^*} + \frac{\partial f}{\partial \beta}\frac{\partial \beta}{\partial \mu_R^*}]_m \frac{\partial \mu_R^*}{\partial \Delta L} + [\frac{\partial f}{\partial a}\frac{\partial a}{\partial \gamma}\frac{\partial \gamma}{\partial \epsilon_R^*} + \frac{\partial f}{\partial \beta}\frac{\partial \beta}{\partial \epsilon_R^*}]_m \frac{\partial \mu_R^*}{\partial \Delta L} + \frac{\partial f}{\partial b}\frac{\partial b}{\partial \Delta L} = 0 , \qquad (4.37)$$

$$a_1 \frac{\partial \mu_R^*}{\partial \Delta L} + a_2 \frac{\partial \epsilon_R^*}{\partial \Delta L} + \frac{\partial f}{\partial b}\frac{\partial b}{\partial \Delta L} = 0 , \qquad (4.38)$$

and for the second short-circuit position

$$b_1 \frac{\partial \mu_R^*}{\partial \Delta L} + b_2 \frac{\partial \epsilon_R^*}{\partial \Delta L} + \frac{\partial f}{\partial b}\frac{\partial b}{\partial \Delta L} = 0 . \qquad (4.39)$$

The derivatives can be calculated explicitly to yield

$$\frac{\partial f}{\partial a} = \frac{1 - \beta^2 \tanh \gamma_0 \Delta L}{\tanh \gamma L + \beta \tanh \gamma_0 \Delta L + \beta(1 + \beta \tanh \gamma L \tanh \gamma_0 \Delta L}) - \frac{\tanh \gamma L + \beta \tanh \gamma_0 \Delta L + \beta(1 + \beta \tanh \gamma L \tanh \gamma_0 L)}{(\tanh \gamma L + \beta \tanh \gamma_0 \Delta L + \beta(1 + \beta \tanh \gamma L \tanh \gamma_0 \Delta L)^2} \times (1 + \beta^2 \tanh \gamma_0 \Delta L) , \qquad (4.40)$$

$$\frac{\partial f}{\partial b} = \frac{\beta - \beta^2 \tanh \gamma L}{\tanh \gamma L + \beta \tanh \gamma_0 \Delta L + \beta(1 + \beta \tanh \gamma L \tanh \gamma_0 \Delta L}) - \frac{\tanh \gamma L + \beta \tanh \gamma_0 \Delta L + \beta(1 + \beta \tanh \gamma L \tanh \gamma_0 L)}{(\tanh \gamma L + \beta \tanh \gamma_0 \Delta L - \beta(1 + \beta \tanh \gamma L \tanh \gamma_0 \Delta L)^2} \times (\beta + \beta^2 \tanh \gamma L) , \qquad (4.41)$$

$$\frac{\partial f}{\partial \beta} =$$

$$\frac{\tanh\gamma_0\Delta L - 1 - 2\beta\tanh\gamma L\tanh\gamma_0 L}{\tanh\gamma L + \beta\tanh\gamma_0\Delta L + \beta(1+\beta\tanh\gamma L\tanh\gamma_0\Delta L}) -$$

$$\frac{\tanh\gamma L + \beta\tanh\gamma_0\Delta L + \beta(1+\beta\tanh\gamma L\tanh\gamma_0 L)}{(\tanh\gamma L + \beta\tanh\gamma_0\Delta L - \beta(1+\beta\tanh\gamma L\tanh\gamma_0\Delta L)^2} \times$$

$$(\tanh\gamma_0\Delta L + 1 + 2\beta\tanh\gamma L\tanh\gamma_0\Delta L)\ . \tag{4.42}$$

The following derivatives will be needed in the forthcoming analysis

$$\frac{\partial a}{\partial \gamma} = L\mathrm{sech}^2\gamma L\ , \tag{4.43}$$

$$\frac{\partial \gamma}{\partial L} = \gamma\mathrm{sech}^2\gamma L\ , \tag{4.44}$$

$$\frac{\partial b}{\partial \Delta L} = \gamma_0\mathrm{sech}^2\gamma_0\Delta L\ , \tag{4.45}$$

$$\frac{\partial \beta}{\partial \gamma} = \frac{1}{\mu_R^*\gamma_0}\ , \tag{4.46}$$

$$\frac{\partial \beta}{\partial \mu_R^*} = \frac{\partial \gamma}{\partial \mu_R^*}\frac{1}{\mu_R^*\gamma_0} - \frac{\gamma}{\gamma_0}\frac{1}{\mu_R^{*2}}\ , \tag{4.47}$$

$$\frac{\partial \beta}{\partial \epsilon_R^*} = \frac{\partial \gamma}{\partial \epsilon_R^*}\frac{1}{\epsilon_R^*\gamma_0} - \frac{\gamma}{\gamma_0}\frac{1}{\epsilon_R^{*2}}\ , \tag{4.48}$$

$$\frac{\partial \beta}{\partial \epsilon_R^*} = \frac{\partial \gamma}{\partial \epsilon_R^*}\frac{\partial \beta}{\partial \gamma}\ , \tag{4.49}$$

$$\frac{\partial \beta}{\partial \epsilon_R^*} = \frac{\partial \gamma}{\partial \epsilon_R^*}\frac{1}{\mu_R^*\gamma_0}\ , \tag{4.50}$$

$$\frac{\partial \gamma}{\partial \mu_R^*} = -\frac{\omega^2/c_{vac}^2\epsilon_R^*}{2\gamma}\ , \tag{4.51}$$

$$\frac{\partial \gamma}{\partial \epsilon_R^*} = -\frac{\omega^2/c_{vac}^2\mu_R^*}{2\gamma}\ , \tag{4.52}$$

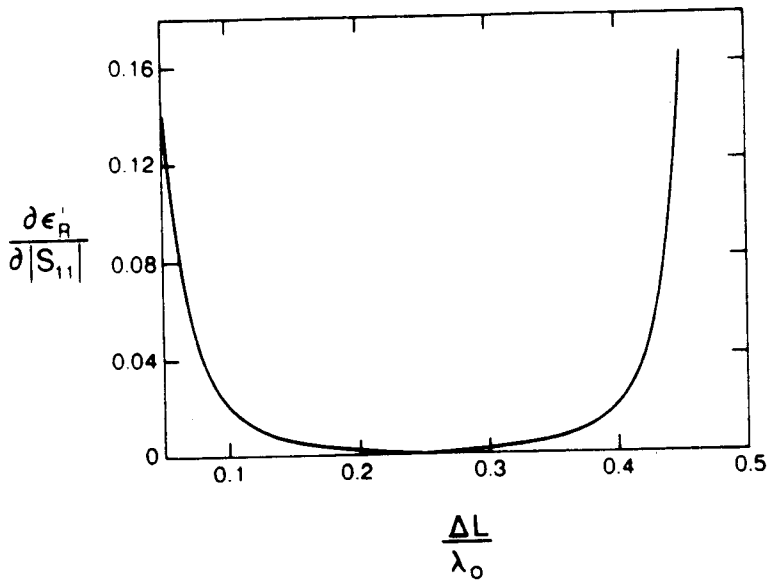

Figure 4.6: A plot of the derivative of ϵ_R' with respect to $|S_{11}|$ as a function of the distance from the short-circuit termination for the case of thin samples $L \ll \lambda_m$.

$$\frac{\partial \mu_R^*}{\partial \theta_i} = -j|S_{11(i)}|\frac{\partial \mu_R^*}{\partial |S_{11(i)}|}\ , \tag{4.53}$$

$$\frac{\partial \mu_R^*}{\partial |S_{11}|} = -\frac{b_2}{b_1}\frac{\partial \epsilon_R^*}{\partial |S_{11(1)}|}\ , \tag{4.54}$$

$$\frac{\partial \epsilon_R^*}{\partial |S_{11(1)}|} = \frac{\exp(j\theta_1)b_1}{a_2b_1 - a_1b_2}\ , \tag{4.55}$$

$$\frac{\partial \mu_R^*}{\partial |S_{11(2)}|} = -\frac{a_2}{a_1}\frac{\partial \epsilon_R^*}{\partial |S_{11(2)}|}\ , \tag{4.56}$$

$$\frac{\partial \epsilon_R^*}{\partial |S_{11(2)}|} = -\frac{\exp(j\theta_2)a_1}{a_2b_1 - a_1b_2}\ . \tag{4.57}$$

In figures 4.6 and 4.7 $\partial \epsilon_R^*/\partial |S_{11}|$ is plotted as a function of the distance from the short circuit termination. We see that in the case of electrically thin samples the minimum uncertainty occurs when the second sample measurement is at $\lambda_0/4$ from the short-circuit termination. As shown in figure 4.7, this is not the case for samples that are not electrically thin.

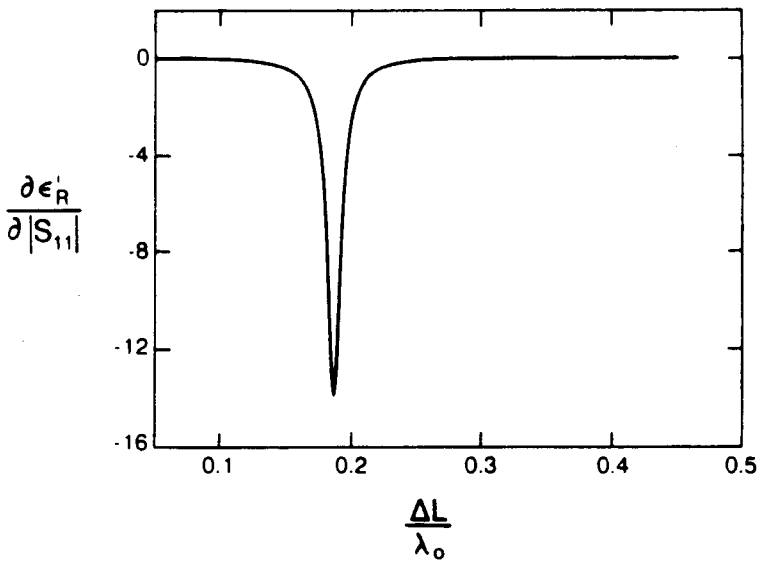

Figure 4.7: A plot of the derivative of ϵ'_R with respect to $|S_{11}|$ as a function of the distance from the short-circuit termination for the case of long samples $L \approx \lambda_m$.